

Review

Corrosion of Laser Cladding High-Entropy Alloy Coatings: A Review

Yusheng Liu ¹, Dingding Xiang ^{1,2,3,*}, Kaiming Wang ^{2,4}  and Tianbiao Yu ^{1,*}¹ School of Mechanical Engineering and Automation, Northeastern University, Shenyang 110057, China² State Key Laboratory of Tribology in Advanced Equipment, Tsinghua University, Beijing 100084, China³ Key Laboratory for Precision and Non-Traditional Machining Technology of Ministry of Education, Dalian University of Technology, Dalian 116081, China⁴ College of Automotive and Mechanical Engineering, Changsha University of Science and Technology, Changsha 410114, China

* Correspondence: xiangdd@mail.neu.edu.cn (D.X.); tbyu@me.neu.edu.cn (T.Y.)

Abstract: Material corrosion is a common phenomenon. Severe corrosion not only causes material failure, but may also lead to unexpected catastrophic accidents. Therefore, reducing the loss caused by corrosion has become a problem faced by countries around the world. As a surface modification technology, laser cladding (LC) can be used to prepare coatings that can achieve metallurgical bonding with the substrate. High-entropy alloys (HEAs) are a new material with superior anti-corrosion ability. Therefore, HEA coatings prepared by LC have become a research hotspot to improve the anti-corrosive ability of material surfaces. In this work, the effects of LC process parameters, post-processing, and the HEA material system on the anti-corrosion ability of HEA coatings and their mechanisms are reviewed. Among them, the LC process parameters influence the anti-corrosion ability by affecting the macroscopic quality, dilution rate, and uniformity of the coatings. The post-processing enhances the anti-corrosion ability of the coatings by improving the internal defects and refining the grain structure. The anti-corrosion ability of the coatings can be improved by appropriately adding transition metal elements such as Ni, Cr, Co, and rare earth elements such as Ce and Y. However, the lattice distortion, diversification of phase composition, and uneven distribution caused by excess elements will weaken the corrosion protection of the coatings. We reviewed the impact of corrosion medium on the anti-corrosion ability of coatings, in which the temperature and pH value of the corrosion medium affect the quality of the passive film on the surface of the coatings, thereby affecting the anti-corrosion ability of the coatings. Finally, to provide references for future research, the development trend of preparing HEA coatings by LC technology is prospected.

Keywords: laser cladding; high-entropy alloys; corrosion resistance; coating preparation

Citation: Liu, Y.; Xiang, D.; Wang, K.; Yu, T. Corrosion of Laser Cladding High-Entropy Alloy Coatings: A Review. *Coatings* **2022**, *12*, 1669. <https://doi.org/10.3390/coatings12111669>

Academic Editor: Alessandro Latini

Received: 27 September 2022

Accepted: 26 October 2022

Published: 3 November 2022

Publisher's Note: MDPI stays neutral with regard to jurisdictional claims in published maps and institutional affiliations.



Copyright: © 2022 by the authors. Licensee MDPI, Basel, Switzerland. This article is an open access article distributed under the terms and conditions of the Creative Commons Attribution (CC BY) license (<https://creativecommons.org/licenses/by/4.0/>).

1. Introduction

With the progress of society, more and more countries have realized the importance of marine economy. However, equipment is prone to corrosion in seawater environments. Severe corrosion will not only lead to material failure and economic loss, but may even endanger human life. Therefore, corrosion protection is related to safety, economy, people's livelihood, ecology, and conservation. As early as the last century, the total direct cost of corrosion in the United States was estimated to be USD 276 billion per year [1]. It is thus urgent to improve the anti-corrosion ability of materials. Surface technology is the use of chemical and physical technologies to modify the surface structure or composition of materials. It can prolong the service life of components and enhance their surface properties, while reducing corrosion costs. As a new star in the material field, high-entropy alloys (HEAs) are also called multi-principal alloys. Compared with traditional alloys, HEAs have four core characteristics [2]: a thermodynamically high entropy effect, a structural lattice distortion effect, a kinetics slow diffusion effect, and a performance

“cocktail” effect. Therefore, HEAs have exceptional properties such as good strength [3], wearability [4], anti-corrosion [5], and resistance to oxidation at high temperatures [6]. HEAs are frequently employed in aerospace, nuclear fusion, and other industries [7]. Scholars typically favor HEAs as surface modification materials. Physical vapor deposition, chemical vapor deposition, laser surface alloying, and laser cladding are some of the current techniques used to prepare HEA coatings. High energy density, adjustable dilution rate, quick processing speed, good metallurgical bonding with the matrix, high solidification rate, and a variety of cladding materials are all advantages of LC over previous preparation techniques [8,9]. LC is frequently employed in functional coating preparation [10] and part repair [11].

Generally, the uniformity of element distribution of materials has a significant influence on the anti-corrosion ability of coatings, and LC technology has the advantage that the coating material can be uniformly clad on the surface of the substrate, and the segregation of elements in the coatings can be easily avoided. The choice of coating material is also one of the factors affecting the anti-corrosion of the coatings, and one of the HEAs’ characteristics is that several kinds of elements can be selected as the main element of the alloy. Due to the high entropy effect of HEAs, their phase composition is relatively simple, and it is not easy to form intermetallic compounds [12,13], and due to its “cocktail” effect, elements with exceptional anti-corrosion ability can be selected to match each other and improve the anti-corrosion ability of the alloys. Using LC technology to prepare HEA coatings can organically combine both advantages and significantly enhance the anti-corrosion ability of the coatings.

At present, the research and application of laser cladding high-entropy alloy coatings (LC-HEACs) in the field of corrosion protection are still in the early stage. In this paper, taking LC-HEACs as the research object, the research status of LC-HEACs in the field of corrosion protection is reviewed and the current research insufficiency and future development trends are pointed out, providing a certain reference for the future development of LC-HEACs in the field of corrosion protection.

2. Influence of LC Process Parameters

Regardless of the production process, it is crucial to optimize the process parameters to achieve the best performance [14,15]. In the LC process, high-energy laser beam radiation is used to melt cladding materials and deposit them on the substrate. To obtain coatings with no macroscopic defects, uniform composition distribution, and exceptional mechanical properties, it is necessary to select appropriate LC process parameters. At present, the effects of laser power, scanning speed, and laser energy density on the anti-corrosion of HEA coatings have been reported.

In general, a smaller molten pool is easily formed by a smaller laser power, which will lead to surface coatings that are melted but substrate that is not melted, so the metallurgical bonding between the substrate and the coatings cannot be achieved. At the same time, too small of a laser power will also lead to many pores in the cladding layer and a large number of cracks between the coatings and the substrate, as shown in Figure 1a. However, the molten pool will be too big if the laser power is too high. In this way, as shown in Figure 1b, the dilution rate will increase, and a large number of elements in the matrix will enter the coatings, decreasing the coatings’ properties as a result.

Qiu et al. [16] successfully prepared Al₂-Co-Cr-Cu-Fe-Ni-Ti HEA coatings with different laser powers by LC technology. The anti-corrosion ability of HEA coatings is the best when the laser power is 2500 W in the corrosive medium of 1 mol/L NaCl solution. When the laser power is low (2000 W), the HEAs are not melted, the cladding layer is not well combined with the substrate, and the corrosion resistance of the HEA coatings decreases. However, when the laser power is higher (3000 W), the matrix is seriously diluted, and a large amount of Fe in the matrix enters the coatings, which weakens the anti-corrosion ability of the coatings.

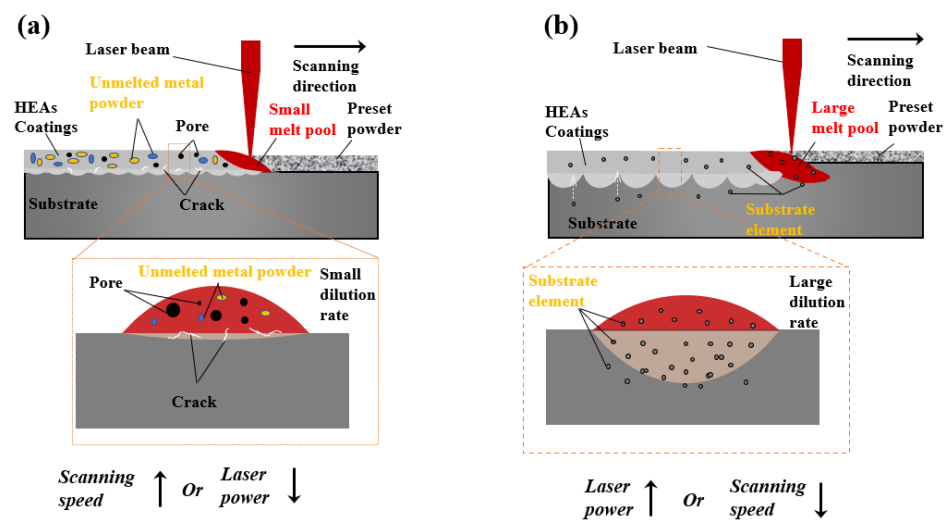


Figure 1. Influence mechanism of laser power and scanning speed on the preparation of HEA coatings: (a) laser power is too small or scanning speed is too fast; (b) laser power is too large or scanning speed is too slow.

The scanning speed has a similar effect to laser power. If the scanning speed is too fast, the coating materials cannot be completely melted, and the effect of cladding cannot be achieved. Meanwhile, with a faster scanning speed, the coatings solidify rapidly, resulting in a large number of structural defects such as pores and cracks in the coatings. However, the molten pool will exist for too long if the scanning speed is too slow, which will lead to the loss of alloy elements due to over-sintering of the coating materials. The increase in heat input is accompanied by the increase in dilution rate and a large number of elements in the matrix will enter the coatings, which will weaken the properties of the coatings.

Qiu et al. [17] prepared Al-Cr-Fe-Cu-Co HEA coatings with different scanning speeds. XRD results demonstrated that the HEA coatings are composed of BCC and FCC phases. Meanwhile, in solutions of 0.5 mol/L H_2SO_4 and 1 mol/L NaCl, electrochemical experiments were conducted. The results show that with the rise in scanning speed, the corrosion potential of the coatings will increase and then decrease, and the corrosion current will decrease and then increase. The reason is that with the increase in scanning speed and when it is appropriate, the time for the laser beam to irradiate the coatings becomes shorter, and the molten pool cools rapidly and produces fine dendrites, which is conducive to grain refinement. This will be beneficial to the improvement of corrosion performance. However, if the scanning speed is too quick, the molten pool is too small, the convection in the molten pool increases, the surface of the coatings is rough, and the anti-corrosion ability is weakened.

Laser energy density (E) is not a direct parameter in LC process parameters, and can be obtained by the formula $E = P/(DV)$. In this formula, P represents laser power, V represents scanning speed, and D represents laser spot size. He et al. [18] prepared a series of Fe-Cr-Ni-Mn-Al HEA coatings by changing the value of E (50~70 J/mm²). The results show that the macro appearance of the coatings changes with the increase in E , and the anti-corrosion ability of the coatings increases first and then decreases. The reason is that the appropriate E value (65 J/mm²) can effectively improve the structural defects and optimize the grain structure in the coatings, thereby enhancing the anti-corrosion ability of the coatings. In addition to laser power, scanning speed, and laser energy density, the LC process also includes important process parameters such as shielding gas rate, defocus distance, powder feeding rate, laser spot size, and overlap ratio. The selection of these process parameters also affects the structure and properties of the HEA coatings. However, there are few reports on the relevant research in this field at present. Therefore, in future study, it is necessary to fully reveal the influence of LC process parameters on the HEA coatings.

3. Influence of Post-Processing Technology

By selecting appropriate process parameters, the defects of the HEA coatings can be effectively reduced, and the anti-corrosion ability of the HEA coatings can be improved. Recently, numerous scholars have also prepared HEA coatings with better properties by combining post-processing technology.

Ultrasonic surface mechanical rolling treatment (USMRT) can form gradient nanostructures in the surface layer, refine grains, and generate compressive residual stress. Cui et al. [19] prepared Fe-Co-Ni-Cr-Mn HEA coatings by LC technology, and applied USMRT to the coatings. The process of LC-HEACs and USMRT was described in Figure 2. After USMT, the grain of the coatings is refined, and the internal stress that inhibits the growth of the coatings' oxide film is effectively reduced by generating compressive residual stress, which greatly enhances the stability of the oxide film and improves the anti-corrosion ability of the coatings.

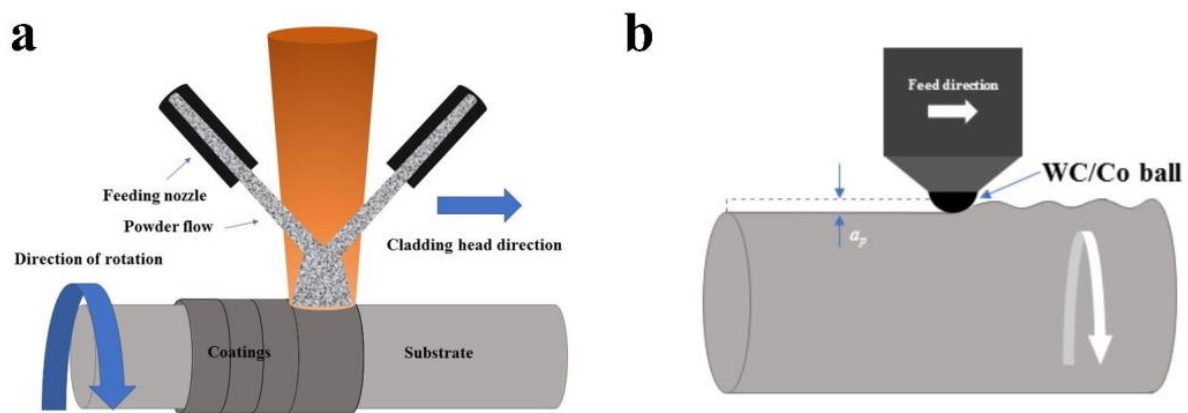


Figure 2. (a) Schematic of LC-HEACs and (b) ultrasonic surface mechanical rolling treatment. Reprinted with permission from [19] 2020 Elsevier.

Ultrasonic impact treatment (UIT) is also a post-processing technology that forms nanocrystals and a work-hardened layer through high strain rate compressive plastic deformation. Figure 3 shows a schematic diagram of the comparison between LC-HEACs and UIT layers. Due to the high strain rate produced by the UIT, the matrix's plastic deformation causes the grain borders and gaps to close and the size of the precipitates between the grain boundaries to shrink, effectively inhibiting intergranular corrosion of the coatings [20]. Li et al. [21] performed UIT on the cladding layer after preparing the $Al_{0.5}$ -Co-Cr-Fe-Mn-Ni HEA coatings. The experimental results show that the coatings after UIT have exceptional anti-corrosion ability. The reason is that the precipitation at the grain boundary of the cladding layer after UIT will be broken into fine precipitates, and at the same time, due to the high strain rate produced by the UIT, the cladding layer's plastic deformation causes the narrowing of the gaps, the grain boundaries to close, and the further reduction in the size of the precipitates, thereby improving the anti-corrosion ability of the coatings.

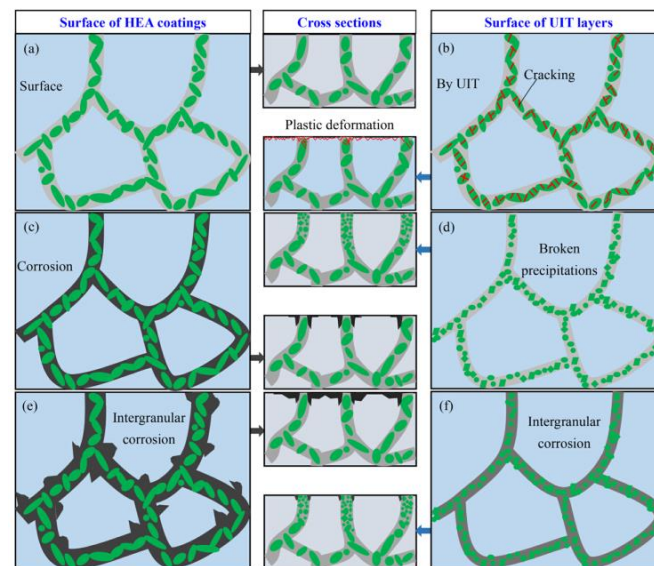


Figure 3. Diagrammatic comparison of the UIT layers and HEA coatings. (a) Surface of HEA coatings; (b) surface of UIT layers; (c) HEA coating is corroded; (d) fractured precipitations and narrower grain boundaries; (e) substantial intergranular corrosion of HEA coatings; (f) mild intergranular corrosion of UIT layers. Reprinted with permission from [21] 2021 Elsevier.

4. Influence of Alloying Elements

As described in Section 2, after selecting appropriate LC process parameters, HEA coatings with a defect-free macrostructure, uniform microstructure, and exceptional anti-corrosion ability can be prepared. The requirements for anti-corrosion of the coatings cannot be fully met only by optimizing LC process parameters, so a large number of scholars improve the anti-corrosion of the coatings by adjusting the types of HEAs in LC-HEACs. Initially, scholars usually studied the corrosion resistance of LC-HEACs with equal or approximate equal molar ratio, such as the Fe-Co-Ni-Cr system composed of transition elements [22] and the Ti-Nb-Zr-Mo system composed of high melting point elements [23], and found that the coatings have adequate anti-corrosion ability. The influence of different material systems on the anti-corrosion ability of the coatings is shown in Table 1. With the development of LC-HEACs, more LC-HEACs with unequal molar ratios have been discovered and reported, and many scholars have begun to research the influence of different elements on the anti-corrosion ability of coatings. This section summarizes the influence of different elements on the anti-corrosion ability of LC-HEACs, which is intended to provide reference for future research.

4.1. Chromium

One of the best components for improving anti-corrosion ability is Cr, which can create a thick layer of Cr_2O_3 oxide on the surface of coatings. Jiang et al. [40] investigated the influence of different Cr additions on the anti-corrosion ability of Al-Co-Cr_x-Fe-Ni ($x = 0.5, 0.75, 1.0, 1.5, 2.0$) LC-HEACs. The findings of the experiments demonstrate that as the amount of Cr added increases, coatings' anti-corrosion ability initially rises and then falls. Adding the appropriate amount of Cr element is conducive to the formation of continuous and uniform passivation film of the coatings, effectively protecting the coatings from corrosion. However, the excess Cr element leads to the dispersion of the oxide layer, which reduces the anti-corrosion ability of the coatings.

Table 1. Effects of different material systems on the corrosion resistance of LC-HEACs.

HEAs	Substrate	Corrosive Medium Solution	Electrochemical Parameters of the Substrate		Electrochemical Parameters of HEA Coatings		Ref.
			E_{corr} (V)	I_{corr} (A/cm ²)	E_{corr} (V)	I_{corr} (A/cm ²)	
-	-	-	E_{corr} (V)	I_{corr} (A/cm ²)	E_{corr} (V)	I_{corr} (A/cm ²)	-
Cu _{0.5} NiAlCoCrFeSi	AZ91D	3.5 wt % NaCl	-1.46	6.20×10^{-4}	-0.76	3.3×10^{-4}	[24]
Cu _{0.9} NiAlCoCrFe	AZ91D	3.5 wt % NaCl	-1.46	6.20×10^{-4}	-1.40	2.56×10^{-8}	[25]
Al _{0.5} CoCrCuFeNi	AZ91D	3.5 wt % NaCl	-1.46	6.20×10^{-4}	-0.998	1.60×10^{-4}	[26]
AlCrFeNiCuCo	Aluminum alloy	1 mol/L H ₂ SO ₄	-0.596	8.056×10^{-5}	-0.493	5.253×10^{-5}	[27]
AlCoCrFeNiTi	AISI1045 steel	1 mol/L NaCl	-0.793	2.98×10^{-6}	-0.470	7.09×10^{-7}	[28]
Al ₂ CoCrFe _{2.7} MoNi	Pure iron	3.5 wt % NaCl	N/A	N/A	0.586	2.762×10^{-9}	[29]
AlCrFeNiCu+5 at % Nb	316 SS	0.5 M H ₂ SO ₄	N/A	N/A	-0.020	9.58×10^{-5}	[30]
AlCoCrFeNiCu	Q235 steel	3.5 wt % NaCl	-0.825	2.482×10^{-5}	-0.061	2.56×10^{-7}	[31]
FeCrNiMnAl	17-4PH stainless steel	3.5 wt % NaCl	-0.860	1.082×10^{-4}	-0.688	1.156×10^{-5}	[18]
CoCrFeNiTi	40CrNiMoA alloy steel	1 mol/L NaCl	-0.70	2.12×10^{-6}	-0.37	1.62×10^{-6}	[32]
AlCoCrFeNiSi	AISI 304 stainless steel	3.5% NaCl	-0.482	7×10^{-6}	-0.326	6.48×10^{-7}	[33]
Ti _{0.8} CrFeCoNiCu	Aluminum alloy	3.5% NaCl	-1.296	1.93×10^{-5}	-0.432	5.12×10^{-7}	[34]
Al ₂ CoCrCuFeNiTi ₂	Q235 steel	0.5 mol/L HCl	-0.41	2.1×10^{-6}	-0.35	1.7×10^{-7}	[35]
Al ₂ CrFeCo ₂ CuNiTi	Q235 steel	0.5 mol/L HNO ₃	-0.35	2.4×10^{-4}	-0.05	2.9×10^{-5}	[5]
Co-Cr-Fe-Ni-Mo _{0.2}	Ti6Al4V	3.5 wt % NaCl	-0.594	9.9×10^{-8}	-0.329	9.87×10^{-8}	[36]
AlCoCrFeNiCu	N/A	3.5 wt % NaCl	N/A	N/A	-0.7019	7.21×10^{-8}	[37]
AlCoCrFeNiTi	N/A	3.5 wt % NaCl	N/A	N/A	-0.4654	7.63×10^{-8}	[37]
CrFeNiNbTi	40CrNiMoA alloy steel	3.5 wt % NaCl	-0.702	2.12×10^{-6}	-0.555	3.58×10^{-6}	[38]
CoCrFeMnTi _{0.2}	15CrMn Steel	1 mol/L NaCl	-0.6705	4.889×10^{-6}	-0.4720	3.408×10^{-6}	[39]

4.2. Nickel

Ni element is also one of the most effective elements for improving the anti-corrosion ability of alloys. Usually, Ni element and Cr element cooperate with each other, which can significantly improve the anti-corrosion ability of the coatings. In 1 mol/L NaOH solution and 3.5 wt % NaCl solution, Qiu et al. [41] investigated the corrosion characteristics of Al₂-Cr-Fe-Co-Cu-Ti-Ni_x ($x = 0, 0.5, 1, 1.5, 2.0$) LC-HEACs. The anti-corrosion ability of the coatings increased initially and then dropped as Ni content increased. Despite the anti-corrosion ability of the Ni element, when the Ni content is high, the alloy suffers from significant lattice distortion, which has an impact on the microstructure and reduces the coatings' anti-corrosion ability.

4.3. Molybdenum

As one of the most effective elements to improve corrosion resistance, Mo is usually combined with Ni and Cr elements [42,43], which are beneficial to improving the anti-corrosion ability of coatings. Fu et al. [44] investigated the influence of different Mo additions on Co-Cr₂-Fe-Ni-Mo_x ($x = 0, 0.1, 0.2, 0.3, 0.4$) LC-HEACs. The findings demonstrate that adding the right amount of Mo can increase the coatings' anti-corrosion ability, but adding too much Mo encourages the development of inter-dendritic structures and the σ -CrMo phase, which speeds up galvanic corrosion and lowers the coatings' anti-corrosion ability. Meanwhile, to further investigate the actual anti-corrosion ability of coatings, a 6-month immersion test was carried out on HEA coating samples and 2605 N duplex stainless steel (stainless steel specially developed for chlorine-containing solutions) in an acidic solution of pH = 2. The surface of 2605 N duplex stainless steel is covered in numerous pits, and after the Mo element was added, the HEACs were able to efficiently control the size of the pits.

4.4. Aluminum

The density of Al is light, and the Al element can form a dense oxide film to improve the corrosion resistance of the material. As a result, many researchers have chosen the Al element as the central component of HEAs [45,46]. Sun et al. [47] used LC technology to prepare Co-Cr-Fe-Ni-Al_x-Mn_(1-x) ($x = 0, 0.2, 0.4, 0.6, 0.8, 1.0$) HEA coatings with different ratios of Al and Mn elements. The phase structure of the HEA coatings changes with the addition of the Al element from a single FCC phase to a dual phase made up of FCC

and BCC, and lastly into a single BCC phase. With an increase in Al concentration, the anti-corrosion ability of the HEA coatings initially declined suddenly and then slowly increased. The coatings only have one FCC phase when no additional Al element is present, and microstructures with uniform phase structures often have superior anti-corrosion ability. The coatings contain FCC and BCC dual phases when a tiny amount of Al element (0.2 at %) is applied. Corrosion micro-cells are created as a result of the equilibrium potential difference between the FCC phase and the BCC phase, which lowers anti-corrosion ability. The possibility of the Al_2O_3 passivation film forming on the surface of the HEA coatings grows as the addition of Al element increases, which leads to a gradual improvement in the coatings' anti-corrosion ability. When the addition amount of Al element is 1.0 at %, the HEA coatings have a single BCC phase composition. At this time, due to the uniform and single microstructure and the existence of the Al_2O_3 oxide film, the anti-corrosion ability of the coatings is the best.

4.5. Titanium

Ti element has strong passivation ability and exceptional corrosion resistance. Therefore, it has been widely studied by scholars. Table 2 summarizes the influence of different Ti additions on the anti-corrosion ability of LC-HEACs.

Table 2. Effects of different Ti additions on the corrosion resistance of LC-HEACs.

HEAs	Substrate	Corrosive Medium Solution	Electrochemical Parameters of the Substrate		Electrochemical Parameters of HEA Coatings		Ref.
			E_{corr} (V)	I_{corr} (A/cm ²)	E_{corr} (V)	I_{corr} (A/cm ²)	
$\text{Al}_2\text{CrFeNiCoCuTi}_x$ $x = 0, 0.5, 1.0, 1.5, 2.0$	Q235 steel	0.5 mol/L HNO_3	−0.35	2.4×10^{-1}	−0.18 for Ti_0 −0.30 for $\text{Ti}_{0.5}$ −0.33 for $\text{Ti}_{1.0}$ −0.30 for $\text{Ti}_{1.5}$ −0.15 for $\text{Ti}_{2.0}$	3.8×10^{-2} for Ti_0 2.2×10^{-2} for $\text{Ti}_{0.5}$ 7.3×10^{-3} for $\text{Ti}_{1.0}$ 4.4×10^{-3} for $\text{Ti}_{1.5}$ 2.7×10^{-3} for $\text{Ti}_{2.0}$	[48]
$\text{Al}_2\text{CoCrCuFeNiTi}_x$ $x = 0, 0.5, 1.0, 1.5$	Q235 steel	0.5 mol/L H_2SO_4	−0.38	3.6×10^{-5}	−0.32 for Ti_0 −0.40 for $\text{Ti}_{0.5}$ −0.52 for $\text{Ti}_{1.0}$ −0.37 for $\text{Ti}_{1.5}$	4.2×10^{-6} for Ti_0 3.1×10^{-7} for $\text{Ti}_{0.5}$ 2.3×10^{-8} for $\text{Ti}_{1.0}$ 1.1×10^{-7} for $\text{Ti}_{1.5}$	[49]
$\text{Al}_2\text{CoCrCuFeNiTi}_x$ $x = 0, 0.5, 1.0, 1.5$	Q235 steel	3.5% NaCl	−0.57	7.1×10^{-7}	−0.58 for Ti_0 −0.45 for $\text{Ti}_{0.5}$ −0.22 for $\text{Ti}_{1.0}$ −0.63 for $\text{Ti}_{1.5}$	6.3×10^{-7} for Ti_0 6.7×10^{-7} for $\text{Ti}_{0.5}$ 1.7×10^{-8} for $\text{Ti}_{1.0}$ 5.4×10^{-7} for $\text{Ti}_{1.5}$	[49]
CoCrFeNiTi_x $x = 0, 0.2, 0.4, 0.6, 0.8$	45 steel	3.5 wt % NaCl	N/A	N/A	−0.848 for Ti_0 −0.792 for $\text{Ti}_{0.2}$ −0.650 for $\text{Ti}_{0.4}$ −0.509 for $\text{Ti}_{0.6}$ −0.598 for $\text{Ti}_{0.8}$	1.99×10^{-6} for Ti_0 8.13×10^{-7} for $\text{Ti}_{0.4}$ 4.22×10^{-7} for $\text{Ti}_{0.6}$ 5.76×10^{-7} for $\text{Ti}_{0.8}$	[50]
CoCrFeNiTi_x $x = 0.1, 0.3, 0.5, 0.7$	Q235 steel	3.5 wt % NaCl	N/A	N/A	−1.18 for $\text{Ti}_{0.1}$ −1.16 for $\text{Ti}_{0.3}$ −1.13 for $\text{Ti}_{0.5}$ −1.11 for $\text{Ti}_{0.7}$	5.64×10^{-6} for $\text{Ti}_{0.1}$ 4.23×10^{-6} for $\text{Ti}_{0.3}$ 3.81×10^{-6} for $\text{Ti}_{0.5}$ 1.04×10^{-6} for $\text{Ti}_{0.7}$	[51]
$\text{CoCr}_{2.5}\text{FeNi}_2\text{Ti}_x$ $x = 0, 0.5, 1.0$	Q235 steel	Simulated saturated salty water mud solution	−0.902	4.531×10^{-14}	−0.714 for Ti_0 −0.578 for $\text{Ti}_{0.5}$ −0.228 for $\text{Ti}_{1.0}$	3.648×10^{-15} for Ti_0 4.892×10^{-15} for $\text{Ti}_{0.5}$ 1.386×10^{-15} for $\text{Ti}_{1.0}$	[52]

It can be seen from Table 2 that in different corrosive media and HEA material systems, the appropriate addition of Ti element can improve the anti-corrosion ability of HEA coatings. Liu et al. [53] reported the influence of Ti element content on the anti-corrosion ability of $\text{Al-Co-Cr-Fe-Ni-Ti}_x$ ($x = 0, 0.2, 0.4, 0.6, 0.8, 1.0$) LC-HEACs. The experimental results demonstrated that in the HEA coatings, the distribution of each element is uniform and the phase structure composition is relatively single, which inhibits the formation of corrosion micro-cells, and the coatings exhibit exceptional anti-corrosion ability.

4.6. Copper

The Cu element helps FCC solid solution develop and it aggregates readily in the intergranular space to produce a Cu-rich phase, which gives HEAs their favorable characteristics.

Li et al. [54] reported the influence of Cu addition on the microstructure and anti-corrosion ability of $\text{Al}_{0.8}\text{-Cr-Fe-Co-Ni-Cu}_x$ LC-HEACs. The experimental results demonstrated that with the increase in Cu addition, the phase structure of the coatings changes from two BCC phases to two BCC phases and one FCC phase. The anti-corrosion ability of the coatings decreases with the increase in Cu addition. The reason is that the additional Cu element added causes an increase in the Cu-rich phase, which in turn causes a rise in the intergranular corrosion area, which causes the contact area between the corrosion solution and the coating surface to continuously grow. As a result, the electrode reaction's coating corrosion rate is accelerated, and the coatings' corrosion resistance is decreased.

4.7. Tantalum

Zhang et al. [55] reported the influence of Ta amount on the microstructure and anti-corrosion ability of Ni-Ti-Cr-Nb-Ta_x ($x = 0.1, 0.3, 0.5, 1$) LC-HEACs. The results show that the formation of BCC phase and the precipitation of Laves phase (Cr_2Nb) are promoted with the increase in Ta element content. In 3.5 wt % NaCl solution, the HEA coatings exhibit exceptional anti-corrosion ability, especially the $\text{Ni-Ti-Cr-Nb-Ta}_{0.5}$ and Ni-Ti-Cr-Nb-Ta coatings, which have a wider passivation zone and show better pitting corrosion resistance.

4.8. Carbon

To report the influence of C on the anti-corrosion of LC-HEACs, Shang et al. [56] prepared $\text{Al}_{6.25}\text{-Mo}_{6.25}\text{-Ti}_{29.2}\text{-Zr}_{29.2}\text{-Nb}_{29.2} + x\text{C}$ at % ($x = 0, 0.4, 0.8$) LC-HEACs on the surface of pure titanium alloy. The distribution of the elements in the HEA coatings becomes more uniform with the proper addition of C, which significantly increases the coatings' anti-corrosion ability. However, when the amount of C is too high, the HEACs are made of BCC solid solution, MC carbide, and HCP- α phase, which speeds up corrosion by causing the development of micro-cells and decreases the anti-corrosion ability of the HEA coatings.

4.9. Ceramic Reinforcement

Many scholars have found that the anti-corrosion ability of LC-HEACs can be effectively improved by introducing reinforcing phases. Table 3 summarizes the effect of enhancing the anti-corrosion ability of relative LC-HEACs. Guo et al. [57] prepared in situ TiN ceramic particles which improved $\text{Co-Cr}_2\text{-Fe-Ni-Ti}_x$ ($x = 0, 0.5, 1$) LC-HEACs. According to the experimental findings, the HEA coatings' phase structure is composed primarily of FCC + TiN with a trace amount of Laves phase. The appropriate addition of Ti element, which can dissolve in the FCC phase to improve the anti-corrosion ability of the HEA coatings, results in the higher positive corrosion potential and lower corrosion current density of the HEA coatings. However, an excessive amount of Ti will result in TiN particles and Laves phase, which will create corrosion micro-cells and heighten the susceptibility to corrode. Liu et al. [58] prepared $\text{Fe-Co-Ni-Cr-Mn-Ti}_x$ ($x = 0, 0.5, 1.0, 1.5$) HEA coatings by LC technology under the protection of nitrogen. Electrochemical experiments show that the coating corrosion potential is high and its corrosion current is low when the addition amount of Ti is 0. With the increase in Ti addition, TiN ceramic particles and Laves phase were formed in situ in the HEA coatings. Due to the different electrode potentials, micro-cells will appear between both the TiN particles and the Laves phase and γ -phase, resulting in galvanic corrosion and weakening the anti-corrosion ability of the HEA coatings.

Table 3. Effect of enhanced relative LC-HEACs' corrosion resistance.

Substrate	HEAs	Enhancement Phase	Corrosive Medium	Electrochemical Parameters of the Substrate		Electrochemical Parameters of HEA Coatings		Ref.
				E_{corr} (V)	I_{corr} (A/cm ²)	E_{corr} (V)	I_{corr} (A/cm ²)	
-	-	-	-	E_{corr} (V)	I_{corr} (A/cm ²)	E_{corr} (V)	I_{corr} (A/cm ²)	-
45 steel	FeCoCrNiCu + Cf	Cf	5% H ₂ SO ₄	-0.437	2.317×10^{-2}	-0.087	2.371×10^{-4}	[59]
304SS	CoCrNiMo + 1 at % B ₄ C	B ₄ C	3.5 wt % NaCl	-0.289	2.21×10^{-7}	-0.255	1.86×10^{-7}	[60]
304SS	CoCrNiMo + 2 at % B ₄ C	B ₄ C	3.5 wt % NaCl	-0.289	2.21×10^{-7}	-0.292	1.82×10^{-7}	[60]
304SS	CoCrNiMo + 3 at % B ₄ C	B ₄ C	3.5 wt % NaCl	-0.289	2.21×10^{-7}	-0.265	2.22×10^{-7}	[60]
304SS	CoCrNiMo + 4.2 at % B ₄ C	B ₄ C	3.5 wt % NaCl	-0.289	2.21×10^{-7}	-0.199	2.84×10^{-7}	[60]
AZ91D	Ti ₅₀ Zr ₂₅ Al ₁₅ Cu ₁₀ + 2 wt % LaB ₆	LaB ₆	3.5 wt % NaCl	-1.37	5.31×10^{-4}	-0.42	1.48×10^{-6}	[61]
AZ91D	Ti ₅₀ Zr ₂₅ Al ₁₅ Cu ₁₀ + 4 wt % LaB ₆	LaB ₆	3.5 wt % NaCl	-1.37	5.31×10^{-4}	-0.34	8.52×10^{-7}	[61]
AZ91D	Ti ₅₀ Zr ₂₅ Al ₁₅ Cu ₁₀ + 8 wt % LaB ₆	LaB ₆	3.5 wt % NaCl	-1.37	5.31×10^{-4}	-0.65	1.14×10^{-5}	[61]
AISI1045 steel	Al _{0.5} CoCrFeNiTi _{0.5} + 2 at % SiC	SiC	3.5 wt % NaCl	N/A	N/A	-0.787	2.116×10^{-8}	[62]
AISI1045 steel	Al _{0.8} CoCrFeNiTi _{0.2} + 2 at % SiC	SiC	3.5 wt % NaCl	N/A	N/A	-0.573	1.005×10^{-8}	[62]
304SS	FeCoNiCrMnTi _{0.5}	In situ TiN	3.5% NaCl	-0.217	5.45×10^{-9}	-0.209	1.15×10^{-10}	[58]
304SS	FeCoNiCrMnTi	In situ TiN	3.5% NaCl	-0.217	5.45×10^{-9}	-0.247	3.18×10^{-10}	[58]
304SS	FeCoNiCrMnTi _{1.5}	In situ TiN	3.5% NaCl	-0.217	5.45×10^{-9}	-0.412	3.965×10^{-8}	[58]
904L stainless steel	CoCr ₂ FeNiTi _{0.5}	In situ TiN	Simulated phosphoric acid reactor solution	-0.213	3.3×10^{-7}	-0.307	3.3×10^{-10}	[57]
904L stainless steel	CoCr ₂ FeNiTi	In situ TiN	Simulated phosphoric acid reactor solution	-0.213	3.3×10^{-7}	-0.231	2.7×10^{-8}	[57]

4.10. Rare Earth Elements

As beneficial chemical and physical modifiers, rare earth elements and their oxides are referred to as the “vitamins of metals”. Cui et al. [63] successfully prepared Fe-Co-Ni-Cr-Mo LC-HEACs with an appropriate amount of CeO₂ on the surface of titanium alloys. Electrochemical studies in a solution of 3.5% NaCl revealed that the addition of CeO₂ increased the corrosion protection of the HEA coatings. The electrochemical corrosion mechanism of HEA coatings and those augmented with CeO₂ in 3.5% NaCl solution is shown in Figure 4. A higher density and more stable passivation film is formed as a result of the addition of CeO₂ powder, which also refines the coating's grain structure, adds more nucleation points for the passivation film to form, and improves the passivation film's uniformity and formation rate. This increases the coatings' resistance to corrosion.

Due to Ce element's exceptional qualities, Y element, another rare earth element, has also captured the interest of academics. The corrosion protection of Mg-Mo-Nb-Fe-Ti₂-Y_x ($x = 0, 0.4, 0.8, 1.2$) LC-HEACs was examined by Gu et al. [64] in relation to the effects of various Y element levels. The results demonstrated that the added Y element improves the corrosion resistance of the HEA coatings, as evidenced by the higher corrosion potential and lower corrosion current density compared to the HEA coatings without the addition of Y element. When Y element is added, structural flaws such microcracks in HEA coatings are somewhat reduced, and Cl⁻ ion entry into the coatings is blocked, which significantly increases HEA coatings' corrosion protection. The amount of Y supplied does not, however, positively correlate with the anti-corrosion ability of HEA coatings. The alloying of Ti and Mo elements, increased lattice distortion, and decreased corrosion protection of HEA coatings are all effects of adding too much Y.

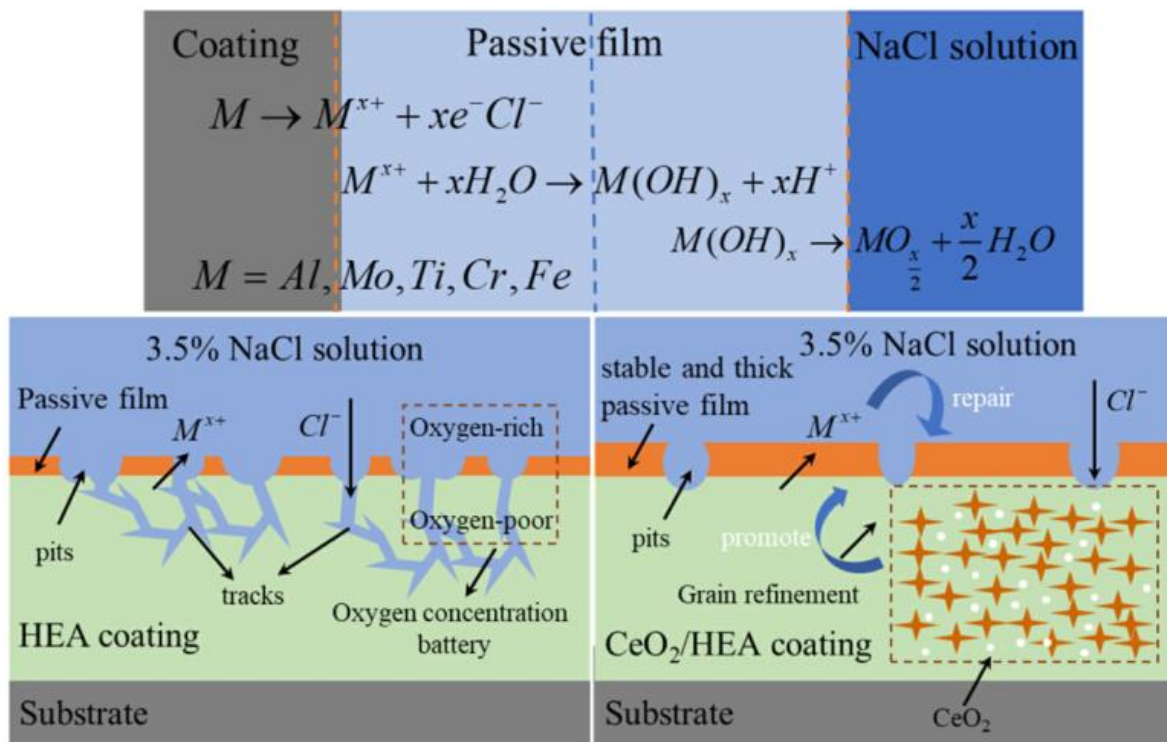


Figure 4. Schematic diagram of corrosion in 3.5% NaCl solution. Reprinted with permission from [63] 2021 Elsevier.

5. Influence of Corrosive Environment

In general, the coating material system, microstructure, and external environment coming into contact with the coatings are the elements that influence the corrosion of metal coatings. Among these, the impact of the coating's microstructure and material system on its anti-corrosion ability has been thoroughly discussed. The corrosion environment, including temperature, humidity, and pH, greatly affects the corrosion performance of the coating. According to current reports, the influence of acid, alkaline, salt solution, room temperature environment, and non-room temperature environment on the performance of HEAs has been reported by scholars. The effects of salt environment (pH = 7) and acid environment (pH < 7) at different temperatures on the corrosion resistance of HEA coatings are shown in Tables 4 and 5, respectively.

The pH value of the corrosive liquid has a considerable influence on the corrosion resistance of the coatings. Qiu et al. [65,66] discussed the effects of acidic environment (pH < 7), alkaline environment (pH > 7), and salt environment (pH = 7) on the corrosion properties of Al₂-Cr-Fe-Co_x-Cu-Ni-Ti HEA coatings. It was found that the corrosion potential and corrosion current of the same HEA coatings were greatly affected under the corrosion environment with different pH values. At the same time, the report also found that there were some differences in corrosion resistance of different HEA material systems under the same corrosion solution, which also confirmed the content of the Section 4 of this paper. Therefore, the pH value of the corrosion solution and the material composition of HEAs significantly affect the corrosion performance of the coatings. Hao et al. [67] explained why it is difficult to form a passive film on the surface of Co-Cr-Fe-Mn-Ni HEAs in a chloride containing salt environment, and proposed an effective method to solve this problem. The alloys are given a nitriding treatment to cause N to react with H⁺ ions in the corrosion medium, with H⁺ ions preventing Mn and Co elements from creating the passive film, thus improving the alloy's capacity to produce the passive film and boosting its anti-corrosion ability.

The temperature of the corrosion medium also affects the corrosion resistance of the alloy. Wang et al. [68] reported the influence of different corrosion solutions (3.5 wt % NaCl

and 0.5 M H₂SO₄) and the external environment at different temperatures on the corrosion performance of Cr-Fe-Co-Ni HEA coatings. The results show that the corrosion potential and corrosion current of the coating worsen and the corrosion resistance of the coating is weakened to a certain extent with the increase in temperature under the same corrosion solution. At the same time, the report also found that the influence of temperature on the corrosion performance of the coating was different in different corrosion solutions. Xue et al. [69] reported the corrosion behavior of Al₂-Cr₅-Cu₅-Fe₅₃-Ni₃₅ HEAs at different temperatures and chloride solution concentrations. The report pointed out that at low temperatures (<25 °C), the coating has exceptional corrosion resistance due to the existence of the oxide film. However, with the increase in temperature, the passive film of the coating is damaged, resulting in accelerated corrosion of the coating. Similarly, higher chloride concentration solutions will considerably weaken the corrosion resistance of the coating.

At present, more and more engineering structural materials need to be used in complex working conditions. Therefore, in addition to the corrosion performance of LC-HEACs in standard acidic, alkali, and salt environments, the corrosion resistance of LC-HEACs in simulated actual working conditions is more valuable. The 20 G steel used in the boiler water-cooling environment is often used in a high-temperature and H₂S-containing environment, which will lead to serious corrosion of the 20 G steel and even a tube burst accident. To solve this problem, Liu et al. [70] prepared Ni-Cr-Mo-W-Si_x LC-HEACs with different Si additions on the surface of 20 G steel, and corrosion experiments were carried out on the HEA coatings in a simulated high-temperature (500–600 °C) H₂S environment. The experimental findings demonstrate the superior anti-corrosion ability of HEA coatings, and particularly when the Si concentration is 1.0 wt %, a protective oxide film forms on the coating's surface to further increase the anti-corrosion ability. However, if Si is added in excess, it can result in large cracks along grain boundaries and poor anti-corrosion ability. Low-carbon steel is widely used in engineering due to its low price. However, the poor corrosion resistance of low-carbon steel seriously affects its service life. Andri Isak Thorhallsson et al. [71] successfully prepared Co-Cr-Fe-Ni-Mo_{0.85} and Al_{0.5}-Co-Cr-Fe-Ni HEA coatings on the surface of low-carbon steel, and tested the anti-corrosion ability of the coatings under three actual geothermal environments. The results show that the corrosion environment has a significant impact on the anti-corrosion ability of the coatings, especially when the HEA coatings have manufacturing defects, as it will further aggravate the corrosion of the coatings. X70 pipeline steel has suitable strength and toughness, as well as weldability, and is widely used in the petroleum industry. However, in the long-term service process, it is easily corroded, resulting in oil leakage, economic losses, and even endangering the personal safety of workers. Therefore, Wan et al. [72] successfully prepared Al_{0.4}-Co-Cu_{0.6}-Ni-Si_{0.2}-Ti_{0.25} LC-HEACs on the X70 pipeline steel substrate. The anti-corrosion ability of HEA coatings in challenging sulfur-containing conditions was investigated in order to prolong the useful life of X70 pipeline steel. The findings reveal that HEA coatings have higher impedance and impedance modulus than X70 steel, which indicates that HEA coatings have significantly superior anti-corrosion ability than X70 steel. HEA coatings also have a more accurate corrosion potential and lower current density. The thorough results demonstrate that HEA coatings have much greater resistance to corrosion than X70 steel.

Table 4. The effects of 3.5 wt % NaCl (pH = 7) at different temperatures on the corrosion resistance of HEA coatings.

HEAs	Temperature (°C)	Electrochemical Parameters of HEA Coatings		Corrosion Mechanism	Ref.
		E _{corr} (V)	I _{corr} (A/cm ²)		
-	-	-	-	-	-
Cr-Fe-Co-Ni	20	-0.166	7.15×10^{-8}	N/A	[68]
Cr-Fe-Co-Ni	40	-0.190	1.33×10^{-7}	N/A	[68]
Cr-Fe-Co-Ni	60	-0.133	2.99×10^{-7}	N/A	[68]
Cr-Fe-Co-Ni-Mo _{0.2}	N/A	-0.192	1.84×10^{-9}	N/A	[73]
Fe-Co-Cr-Ni-Al	N/A	-0.485	1.29×10^{-5}	N/A	[74]
Fe-Co-Cr _{1.5} -Ni-Al	N/A	-0.297	2.56×10^{-6}	N/A	[74]
Fe-Co-Cr _{2.0} -Ni-Al	N/A	-0.423	6.983×10^{-6}	N/A	[74]
Al _{0.5} -Co-Cr-Fe-Ni-Ti _{0.5}	27	-0.610	9.91×10^{-9}	Pitting corrosion	[62]
Al _{0.5} -Co-Cr-Fe-Ni-Ti _{0.5} +2 at % Si	27	-0.787	2.11×10^{-8}	Pitting corrosion	[62]
Al _{0.8} -Co-Cr-Fe-Ni-Ti _{0.2}	27	-0.509	1.37×10^{-8}	Pitting corrosion	[62]
Al _{0.8} -Co-Cr-Fe-Ni-Ti _{0.2} +2 at % Si	27	-0.573	1.00×10^{-8}	Pitting corrosion	[62]
Fe-Ni-Co-Cr	22~28	-0.188	8.77×10^{-9}	Intergranular corrosion	[43]
Fe-Ni-Co-Cr-Mo _{0.15}	22~28	-0.161	7.63×10^{-9}	Intergranular corrosion	[43]
Fe-Ni-Co-Cr-Mo _{0.2}	22~28	-0.142	3.68×10^{-9}	Intergranular corrosion	[43]
Fe-Ni-Co-Cr-Mo _{0.25}	22~28	-0.192	5.37×10^{-9}	Intergranular corrosion	[43]
Al _{0.3} -Cu _{0.3} -Co-Cr-Fe-Ni	20~24	-0.294~ -0.282	$2.42\sim 3.04 \times 10^{-7}$	Pitting and galvanic corrosion	[75]
Al _{0.3} -Cu _{0.4} -Co-Cr-Fe-Ni	20~24	-0.271~ -0.251	$2.92\sim 3.88 \times 10^{-7}$	Pitting and galvanic corrosion	[75]
Al _{0.3} -Cu _{0.5} -Co-Cr-Fe-Ni	20~24	-0.263~ -0.245	$6.90\sim 7.96 \times 10^{-7}$	Pitting and galvanic corrosion	[75]
Al _{0.3} -Cu _{0.6} -Co-Cr-Fe-Ni	20~24	-0.255~ -0.241	$9.53\sim 9.99 \times 10^{-7}$	Pitting and galvanic corrosion	[75]

Table 5. The effects of acidic environment (pH < 7) at different temperatures on the corrosion resistance of HEA coatings.

HEAs	Medium	Temperature (°C)	Electrochemical Parameters of HEA Coatings		Ref.
			E _{corr} (V)	I _{corr} (A/cm ²)	
-	-	-	-	-	-
Cr-Fe-Co-Ni	0.5 M H ₂ SO ₄	20	-0.737	7.07×10^{-5}	[68]
Cr-Fe-Co-Ni	0.5 M H ₂ SO ₄	40	-0.767	4.97×10^{-4}	[68]
Cr-Fe-Co-Ni	0.5 M H ₂ SO ₄	60	-0.759	1.26×10^{-3}	[68]
Cr-Fe-Co-Ni	0.5 M H ₂ SO ₄	80	-0.758	3.32×10^{-3}	[68]
Cr-Fe-Co-Ni-Mo _{0.2}	1 M H ₂ SO ₄	N/A	-0.406	2.28×10^{-8}	[73]
Cr-Mn-Fe-Co-Ni	0.1 M H ₂ SO ₄	25	-0.509	6.21×10^{-4}	[76]

6. Corrosion Resistance Enhancement Mechanism

The factors affecting metal corrosion include metal material itself and external environment. The metal material itself includes the composition of the metal and the surface finish of the metal material, while the external environment includes the temperature, humidity, and pH value of the contact environment [77–79]. When the external environment cannot be changed, the alloy can be formed by improving the metal structure and selecting elements with exceptional anti-corrosion ability. In fact, LC-HEACs have a suitable coating structure and a flexible selection of coating materials, thus significantly improving the anti-corrosion ability of the substrate surface. The following three reasons (as shown in Figure 5) are primarily responsible for the superior corrosion resistance of LC-HEACs:

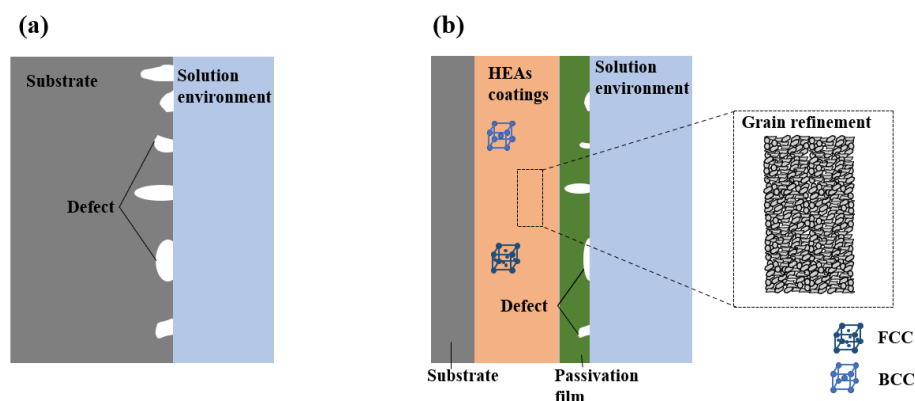


Figure 5. Schematic representation of corrosion resistance mechanism: (a) bare substrate; (b) LC-HEACs.

(1) From the perspective of LC technology: LC technology can produce coatings with exceptional microstructures. Generally, coatings with fine microstructures perform well in anti-corrosion, because this not only reduces the impurity concentration at the grain boundary, but also reduces the component segregation during rapid cooling (Figure 5b).

(2) From the perspective of HEAs: HEAs are composed of a variety of main elements, some of which can react with oxygen in the air, such as Cr, Al, and Mo, to produce a dense Cr_2O_3 , Al_2O_3 , and MoO_2 passivation film on the surface of the HEA coatings (Figure 5b), so that under the protection of passive film, it can effectively prevent corrosion ions from entering and corroding the coatings, which greatly inhibits the damage of the corrosion ions to the coatings and the substrate.

(3) From the perspective of LC-HEACs: LC-HEACs frequently form simple FCC or BCC phase under the circumstances of high mixing entropy impact of various primary components and quick solidification of LC [66,80], which further lessens the development of corroded galvanic cells and reduces the coating's propensity for corrosion.

7. Conclusions

In this work, the influence rule and mechanism of anti-corrosion of LC-HEACs are summarized from four aspects: laser cladding process parameters, post-processing technology, high-entropy alloy material system, and service environment. The corrosion behavior of LC-HEACs was studied in the following ways: (1) electrochemical tests, (2) characterizing and analyzing passive film, and (3) analysis of corrosion morphology and corrosion mechanism. At present, with the research of many scholars, the influence laws and mechanisms of different elements on the anti-corrosion of LC-HEACs have been gradually clarified, and HEA material systems with exceptional corrosion resistance have been discovered. At the same time, various workable approaches to enhance the anti-corrosion ability of LC-HEACs are also proposed. However, it is important to prepare LC-HEACs with greater anti-corrosion ability in order to increase the application range of LC-HEACs in the field of anti-corrosion. The following aspects may be the focus of future investigations.

(1) For different complex engineering practical application environments, design corresponding LC-HEACs as needed, and carry out the corrosion resistance test in the simulated actual service environment to study the anti-corrosion ability of the coatings in the corrosive environment.

(2) Develop a new LC-HEACs material system, e.g., a lightweight LC-HEACs material system composed of light elements such as Al, Mg, or Sc, which is more in line with the trend of lightweight design and manufacturing. To reduce the preparation cost of LC-HEACs, focus on the research of affordable elements to realize the industrialization of LC-HEACs. At the same time, when developing a corrosion-resistant LC-HEACs, it is necessary to take into account the wearability and hardness of the HEA coatings.

(3) At present, there are a few studies on the influence of LC process parameters such as laser power, scanning speed, and laser spot size on the anti-corrosion ability of HEA

coatings. Moreover, the lack of a theoretical model for the primary selection of process parameters leads to unnecessary waste of materials in the process of seeking the best process parameters. Therefore, a general theoretical model for selecting appropriate process parameters should be established in future studies.

(4) Many types of equipment are used in harsh environments. The surface of the equipment is not affected by corrosion alone, but rather the coupling effect of wear and corrosion. Therefore, the exacerbation of corrosion due to wear should be considered in future studies.

Funding: The project was supported by Project Funded by China Postdoctoral Science Foundation (2022M710633), the Liaoning Province Natural Science Foundation (2022-YGJC-79, 2022-BS-078), the Tribology Science Fund of State Key Laboratory of Tribology (SKLTKF21B03), the Science Fund of Key Laboratory for Precision and Non-Traditional Machining Technology of Ministry of Education (B202101) and the Fundamental Research Funds for the Central Universities (N2203017).

Institutional Review Board Statement: Not applicable.

Informed Consent Statement: Not applicable.

Data Availability Statement: Not applicable.

Acknowledgments: The authors thank Northeastern University Zhao Ji for his useful comments and suggestions on this manuscript.

Conflicts of Interest: The authors declare that they have no conflict of interest.

References

1. Koch, G.; Brongers, M.; Thompson, N.; Virmani, Y.; Payer, J. *Corrosion Cost and Preventive Strategies in the United States*; Federal Highway Administration: McLean, VA, USA, 2002.
2. Fu, Y.; Li, J.; Luo, H.; Du, C.; Li, X. Recent advances on environmental corrosion behavior and mechanism of high-entropy alloys. *J. Mater. Sci. Technol.* **2021**, *80*, 217–233. [[CrossRef](#)]
3. Ren, J.; Zhang, Y.; Zhao, D.; Chen, Y.; Guan, S.; Liu, Y.; Liu, L.; Peng, S.; Kong, F.; Poplawsky, J.; et al. Strong yet ductile nanolamellar high-entropy alloys by additive manufacturing. *Nature* **2022**, *608*, 62–68. [[CrossRef](#)] [[PubMed](#)]
4. Li, Y.; Wang, K.; Fu, H.; Guo, X.; Lin, J. Microstructure and wear resistance of in-situ TiC reinforced AlCoCrFeNi-based coatings by laser cladding. *Appl. Surf. Sci.* **2022**, *585*, 152703. [[CrossRef](#)]
5. Qiu, X. Microstructure and corrosion properties of Al₂CrFeCo_xCuNiTi high entropy alloys prepared by additive manufacturing. *J. Alloys Compd.* **2021**, *887*, 161422. [[CrossRef](#)]
6. Li, S.; Yamaguchi, T. High-temperature oxidation behavior of laser-cladded refractory NiSi_{0.5}CrCoMoNb_{0.75} high-entropy coating. *J. Mater. Res. Technol.* **2022**, *17*, 1616–1627. [[CrossRef](#)]
7. Zhang, Y.; Zuo, T.; Tang, Z.; Gao, M.; Dahmen, K.; Liaw, P.; Lu, Z. Microstructures and properties of high-entropy alloys. *Prog. Mater. Sci.* **2014**, *61*, 1–93. [[CrossRef](#)]
8. Zhu, L.; Xue, P.; Lan, Q.; Meng, G.; Ren, Y.; Yang, Z.; Xu, P.; Liu, Z. Recent research and development status of laser cladding: A review. *Opt. Laser Technol.* **2021**, *138*, 106915. [[CrossRef](#)]
9. Chen, L.; Zhao, Y.; Song, B.; Yu, T.; Liu, Z. Modeling and simulation of 3D geometry prediction and dynamic solidification behavior of Fe-based coatings by laser cladding. *Opt. Laser Technol.* **2021**, *139*, 107009. [[CrossRef](#)]
10. Zhao, Y.; Zhang, T.; Chen, L.; Yu, T.; Sun, J.; Guan, C. Microstructure and mechanical properties of Ti-C-TiN-reinforced Ni204-based laser-cladding composite coating. *Ceram. Int.* **2021**, *47*, 5918–5928. [[CrossRef](#)]
11. Chen, L.; Zhao, Y.; Chen, X.; Yu, T.; Xu, P. Repair of spline shaft by laser-cladding coarse TiC reinforced Ni-based coating: Process, microstructure and properties. *Ceram. Int.* **2021**, *47*, 30113–30128. [[CrossRef](#)]
12. Cui, Y.; Shen, J.; Hu, S.; Geng, K. Oxidation and wear mechanisms of FeCoCrNiMnAl_x cladding layers at high-temperature condition. *Coatings* **2020**, *10*, 1136. [[CrossRef](#)]
13. Li, X.; Feng, Y.; Liu, B.; Yi, D.; Yang, X.; Zhang, W.; Chen, G.; Liu, Y.; Bai, P. Influence of NbC particles on microstructure and mechanical properties of AlCoCrFeNi high-entropy alloy coatings prepared by laser cladding. *J. Alloys Compd.* **2019**, *788*, 485–494. [[CrossRef](#)]
14. Chen, Z.; Lu, Y.; Luo, F.; Zhang, S.; Wei, P.; Yan, S.; Wang, Y. Effect of laser scanning speed on the microstructure and mechanical properties of laser-powder-bed-fused K418 nickel-based alloy. *Materials* **2022**, *15*, 3045. [[CrossRef](#)]
15. Yu, H.; Meng, X.; Wang, Z.; Chen, C. Influence of scanning speed on the microstructure and wear resistance of laser alloying coatings on Ti-6Al-4V substrate. *Materials* **2022**, *15*, 5819. [[CrossRef](#)]
16. Qiu, X.; Liu, C. Effect of laser processing parameters on quality of Al₂CoCrCuFeNiTi high-entropy alloys coating. *Mater. Sci. Eng. Powder Metall.* **2015**, *20*, 59–64.

17. Qiu, X.; Zhang, Y.; He, L.; Liu, C. Microstructure and corrosion resistance of AlCrFeCuCo high entropy alloy. *J. Alloys Compd.* **2013**, *549*, 195–199. [[CrossRef](#)]
18. He, R.; Wu, M.; Cui, C.; Miao, X.; Gong, Y. Effects of laser energy density on microstructure and corrosion resistance of FeCrNiMnAl high entropy alloy coating. *Opt. Laser Technol.* **2022**, *152*, 108188.
19. Cui, Z.; Qin, Z.; Dong, P.; Mi, Y.; Gong, D.; Li, W. Microstructure and corrosion properties of FeCoNiCrMn high entropy alloy coatings prepared by high speed laser cladding and ultrasonic surface mechanical rolling treatment. *Mater. Lett.* **2020**, *259*, 126769. [[CrossRef](#)]
20. Zhang, S.; Han, B.; Li, M.; Hu, C.; Zhang, Q.; Liu, X.; Wang, Y. Investigation on microstructure and properties of laser clad AlCoCrCuFeNi high entropy alloy coating by ultrasonic impact treatment. *Intermetallics* **2021**, *128*, 107017. [[CrossRef](#)]
21. Li, M.; Zhang, Q.; Han, B.; Song, L.; Li, J.; Zhang, S. Effects of ultrasonic impact treatment on structures and properties of laser cladding Al_{0.5}CoCrFeMnNi high entropy alloy coatings. *Mater. Chem. Phys.* **2021**, *258*, 123850. [[CrossRef](#)]
22. Yue, T.M.; Zhang, H. Laser cladding of FeCoNiCrAlCu_xSi_{0.5} high entropy alloys on AZ31 Mg alloy substrates. *Mater. Res. Innov.* **2014**, *18* (Suppl. 2), S624–S628. [[CrossRef](#)]
23. Huang, Y.; Wang, Z.; Xu, Z.; Zang, X.; Chen, X. Microstructure and properties of TiNbZrMo high entropy alloy coating. *Mater. Lett.* **2021**, *285*, 129004. [[CrossRef](#)]
24. Yue, T.M.; Huang, K.J. Laser cladding of Cu_{0.5}NiAlCoCrFeSi high entropy alloy on AZ91D magnesium substrates for improving wear and corrosion resistance. *World J. Eng.* **2012**, *9*, 119–124. [[CrossRef](#)]
25. Huang, K.J.; Lin, X.; Wang, Y.Y.; Xie, C.S.; Yue, T.M. Microstructure and corrosion resistance of Cu_{0.9}NiAlCoCrFe high entropy alloy coating on AZ91D magnesium alloys by laser cladding. *Mater. Res. Innov.* **2014**, *18* (Suppl. 2), S1008–S1011. [[CrossRef](#)]
26. Huang, K.; Chen, L.; Lin, X.; Huang, H.; Tang, S.; Du, F. Wear and corrosion resistance of Al_{0.5}CoCrCuFeNi high-entropy alloy coating deposited on AZ91D magnesium alloy by laser cladding. *Entropy* **2018**, *20*, 915. [[CrossRef](#)]
27. Shi, Y.; Ni, C.; Liu, J.; Huang, G. Microstructure and properties of laser clad high-entropy alloy coating on aluminium. *Mater. Sci. Technol.* **2018**, *34*, 1239–1245.
28. Liu, H.; Liu, J.; Chen, P.; Yang, H.; Hao, J.; Tian, X. Microstructure and properties of AlCoCrFeNiTi high-entropy alloy coating on AISI1045 steel fabricated by laser cladding. *J. Mater. Eng. Perform.* **2019**, *28*, 1544–1552. [[CrossRef](#)]
29. Sha, M.; Jia, C.; Qiao, J.; Feng, W.; Ai, X.; Jing, Y.; Shen, M.; Li, S. Microstructure and properties of high-entropy Al_xCoCrFe_{2.7}MoNi alloy coatings prepared by laser cladding. *Metals* **2019**, *9*, 1243. [[CrossRef](#)]
30. Pityana, S.; Malatji, N.; Popoola, A.; Lengopeng, T.; Pityana, S. Effect of Nb addition on the microstructural, mechanical and electrochemical characteristics of AlCrFeNiCu high-entropy alloy. *Int. J. Miner. Metall. Mater.* **2020**, *27*, 1332–1340.
31. Li, L.; Ye, H.; Liu, Y. Process optimization and corrosion resistance of laser cladding AlCoCrFeNiCu high-entropy alloy. *Surf. Technol.* **2022**, *51*, 388–396.
32. Liu, H.; Gao, W.; Liu, J.; Du, X.; Li, X.; Yang, H. Microstructure and properties of CoCrFeNiTi high-entropy alloy coating fabricated by laser cladding. *J. Mater. Eng. Perform.* **2020**, *29*, 7170–7178. [[CrossRef](#)]
33. Zhang, G.; Liu, H.; Tian, X.; Chen, P.; Yang, H.; Hao, J. Microstructure and properties of AlCoCrFeNiSi high-entropy alloy coating on AISI 304 stainless steel by laser cladding. *J. Mater. Eng. Perform.* **2020**, *29*, 278–288. [[CrossRef](#)]
34. Li, Y.; Shi, Y. Phase assemblage and properties of laser clad Ti_xCrFeCoNiCu high-entropy alloy coating on aluminum. *Mater. Res. Express* **2020**, *7*, 36519. [[CrossRef](#)]
35. Qiu, X. Structure and electrochemical properties of laser cladding Al₂CoCrCuFeNiTi_x high-entropy alloy coatings. *Met. Mater. Int.* **2019**, *26*, 998–1003. [[CrossRef](#)]
36. Deng, C.; Wang, C.; Chai, L.; Wang, T.; Luo, J. Mechanical and chemical properties of CoCrFeNiMo_{0.2} high entropy alloy coating fabricated on Ti6Al4V by laser cladding. *Intermetallics* **2022**, *144*, 107504. [[CrossRef](#)]
37. Dada, M.; Popoola, P.; Mathe, N.; Pityana, S.; Adeosun, S.; Aramide, O. The comparative study of the microstructural and corrosion behaviour of laser-deposited high entropy alloys. *J. Alloys Compd.* **2021**, *866*, 158777. [[CrossRef](#)]
38. Zhang, T.; Liu, H.; Hao, J.; Chen, P.; Yang, H. Evaluation of microhardness, tribological properties, and corrosion resistance of CrFeNiNbTi high-entropy alloy coating deposited by laser cladding. *J. Mater. Eng. Perform.* **2021**, *30*, 9245–9255. [[CrossRef](#)]
39. Liu, H.; Li, X.; Liu, J.; Gao, W.; Du, X.; Hao, J. Microstructural evolution and properties of dual-layer CoCrFeMnTi_{0.2} high-entropy alloy coating fabricated by laser cladding. *Opt. Laser Technol.* **2021**, *134*, 106646. [[CrossRef](#)]
40. Jing, Y.; Li, J.; Juan, Y.; Lu, Z.; Jia, W. Evolution in microstructure and corrosion behavior of AlCoCr_xFeNi high-entropy alloy coatings fabricated by laser cladding. *J. Alloys Compd.* **2019**, *775*, 1–14. [[CrossRef](#)]
41. Qiu, X.; Liu, C. Microstructure and properties of Al₂CrFeCoCuTiNi_x high-entropy alloys prepared by laser cladding. *J. Alloys Compd.* **2013**, *553*, 216–220. [[CrossRef](#)]
42. Gu, Z.; Peng, W.; Guo, W.; Zhang, Y.; Hou, J.; He, Q.; Zhao, K.; Xi, S. Design and characterization on microstructure evolution and properties of laser-cladding Ni_{1.5}CrFeTi₂B_{0.5}Mo_x high-entropy alloy coatings. *Surf. Coat. Technol.* **2021**, *408*, 126793.
43. Wu, H.; Zhang, S.; Wang, Z.; Zhan, C.; Chen, H.; Chen, J. New studies on wear and corrosion behavior of laser cladding FeNiCoCrMo_x high entropy alloy coating: The role of Mo. *Int. J. Refract. Met. Hard Mater.* **2022**, *102*, 105721. [[CrossRef](#)]
44. Fu, Y.; Huang, C.; Du, C.; Li, J.; Dai, C.; Luo, H.; Liu, Z.; Li, X. Evolution in microstructure, wear, corrosion, and tribocorrosion behavior of Mo-containing high-entropy alloy coatings fabricated by laser cladding. *Corros. Sci.* **2021**, *191*, 109727. [[CrossRef](#)]
45. Xu, Y.; Li, Z.; Liu, J.; Chen, Y.; Zhang, F.; Wu, L.; Hao, J.; Liu, L. Microstructure evolution and properties of laser cladding CoCrFeNiTiAl_x high-entropy alloy coatings. *Coatings* **2020**, *10*, 373. [[CrossRef](#)]

46. Li, Y.; Shi, Y. Microhardness, wear resistance, and corrosion resistance of $Al_xCrFeCoNiCu$ high-entropy alloy coatings on aluminum by laser cladding. *Opt. Laser Technol.* **2021**, *134*, 106632.
47. Sun, S.; Liu, H.; Hao, J.; Yang, H. Microstructural evolution and corrosion behavior of $CoCrFeNiAl_xMn_{(1-x)}$ dual-phase high-entropy alloy coatings prepared by laser cladding. *J. Alloys Compd.* **2021**, *886*, 161251. [[CrossRef](#)]
48. Qiu, X.; Zhang, Y.; Liu, C. Effect of Ti content on structure and properties of $Al_2CrFeNiCoCuTi_x$ high-entropy alloy coatings. *J. Alloys Compd.* **2014**, *585*, 282–286. [[CrossRef](#)]
49. Qiu, X. Microstructure, hardness and corrosion resistance of $Al_2CoCrCuFeNiTi_x$ high-entropy alloy coatings prepared by rapid solidification. *J. Alloys Compd.* **2018**, *735*, 359–364. [[CrossRef](#)]
50. Zuo, R.; Sun, R.; Niu, W. Microstructure and properties of $CoCrFeNiTi_x$ high entropy alloy coated by laser cladding. *Surf. Technol.* **2022**, *51*, 363–370.
51. Wang, X.; Liu, Q.; Huang, Y.; Xie, L.; Xu, Q.; Zhao, T. Effect of Ti content on the microstructure and corrosion resistance of $CoCrFeNiTi_x$ high entropy alloys prepared by laser cladding. *Materials* **2020**, *13*, 2209. [[CrossRef](#)]
52. Gu, Z.; Xi, S.; Sun, C. Microstructure and properties of laser cladding and $CoCr_{2.5}FeNi_2Ti_x$ high-entropy alloy composite coatings. *J. Alloys Compd.* **2020**, *819*, 152986. [[CrossRef](#)]
53. Liu, J.; Liu, H.; Chen, P.; Hao, J. Microstructural characterization and corrosion behaviour of $AlCoCrFeNiTi_x$ high-entropy alloy coatings fabricated by laser cladding. *Surf. Coat. Technol.* **2019**, *361*, 63–74. [[CrossRef](#)]
54. Li, Y.; Shi, Y.; Olugbade, E. Microstructure, mechanical, and corrosion resistance properties of $Al_{0.8}CrFeCoNiCu_x$ high-entropy alloy coatings on aluminum by laser cladding. *Mater. Res. Express* **2020**, *7*, 26504. [[CrossRef](#)]
55. Zhang, X.; Cui, X.; Jin, G.; Ding, Q.; Zhang, D.; Wen, X.; Jiang, L.; Wan, S.; Tian, H. Microstructure evolution and properties of $NiTiCrNbTa_x$ refractory high-entropy alloy coatings with variable Ta content. *J. Alloys Compd.* **2022**, *891*, 161756. [[CrossRef](#)]
56. Shang, X.; Bo, S.; Guo, Y.; Liu, Q. ZrC reinforced refractory-high-entropy-alloy coatings: Compositional design, synthesis, interstitials, and microstructure evolution effects on wear, corrosion and oxidation behaviors. *Appl. Surf. Sci.* **2021**, *564*, 150466. [[CrossRef](#)]
57. Guo, Y.; Shang, X.; Liu, Q. Microstructure and properties of in-situ TiN reinforced laser cladding $CoCr_2FeNiTi_x$ high-entropy alloy composite coatings. *Surf. Coat. Technol.* **2018**, *344*, 353–358. [[CrossRef](#)]
58. Liu, S.; Zhang, M.; Zhao, G.; Wang, X.; Wang, J. Microstructure and properties of ceramic particle reinforced $FeCoNiCrMnTi$ high entropy alloy laser cladding coating. *Intermetallics* **2022**, *140*, 107402. [[CrossRef](#)]
59. Zhao, M.; Wu, T.; Liu, D.; Huang, Y.; Zhao, L.; Tang, Y.; Shen, M.; Hu, Y.; Zhang, J.; Li, J.; et al. Effect of carbon fiber on microstructure evolution and surface properties of $FeCoCrNiCu$ high-entropy alloy coatings. *Mater. Corros.* **2020**, *71*, 430–439. [[CrossRef](#)]
60. Jiang, D.; Cui, H.; Chen, H.; Zhao, X.; Ma, G.; Song, X. Wear and corrosion properties of B_4C -added $CoCrNiMo$ high-entropy alloy coatings with in-situ coherent ceramic. *Mater. Des.* **2021**, *210*, 110068. [[CrossRef](#)]
61. Jiang, L.; Cui, X.; Jin, G.; Tian, Z.; Wen, X.; Tian, H.; Wang, S. Design and characterization of in-situ TiB reinforced $TiB/Ti_{50}Zr_{25}Al_{15}Cu_{10}$ non-equiatomic medium-entropy alloy composite coating on magnesium alloy by laser cladding. *Opt. Laser Technol.* **2022**, *156*, 108494. [[CrossRef](#)]
62. Xu, Y.; Wang, G.; Song, Q.; Lu, X.; Li, Z.; Zhao, Q.; Chen, Y. Microstructure, mechanical properties, and corrosion resistance of SiC reinforced $Al_xCoCrFeNiTi_{1-x}$ high-entropy alloy coatings prepared by laser cladding. *Surf. Coat. Technol.* **2022**, *437*, 128349. [[CrossRef](#)]
63. Cui, C.; Wu, M.; Miao, X.; Zhao, Z.; Gong, Y. Microstructure and corrosion behavior of $CeO_2/FeCoNiCrMo$ high-entropy alloy coating prepared by laser cladding. *J. Alloys Compd.* **2022**, *890*, 161826. [[CrossRef](#)]
64. Gu, Z.; Mao, P.; Gou, Y.; Chao, Y.; Xi, S. Microstructure and properties of $MgMoNbFeTi_2Y_x$ high entropy alloy coatings by laser cladding. *Surf. Coat. Technol.* **2020**, *402*, 126303. [[CrossRef](#)]
65. Qiu, X.; Wu, M.; Liu, C.; Zhang, Y.; Huang, C. Corrosion performance of $Al_2CrFeCo_xCuNiTi$ high-entropy alloy coatings in acid liquids. *J. Alloys Compd.* **2017**, *708*, 353–357. [[CrossRef](#)]
66. Qiu, X. Corrosion behavior of $Al_2CrFeCo_xCuNiTi$ high-entropy alloy coating in alkaline solution and salt solution. *Results Phys.* **2019**, *12*, 1737–1741. [[CrossRef](#)]
67. Feng, H.; Li, H.; Dai, J.; Han, Y.; Qu, J.; Jian, Z.; Zhan, Y.; Zhan, T. Why $CoCrFeMnNi$ HEA could not passivate in chloride solution?—A novel strategy to significantly improve corrosion resistance of $CoCrFeMnNi$ HEA by N-alloying. *Corros. Sci.* **2022**, *204*, 110396. [[CrossRef](#)]
68. Wang, C.; Yu, Y.; Shao, M.; Zhang, H. Effect of temperature on corrosion behavior of laser-remelted $CrFeCoNi$ coating. *Metals* **2022**, *12*, 970. [[CrossRef](#)]
69. Xue, L.; Ding, Y.; Pradeep, K.; Case, R.; Castaneda, H.; Paredes, M. Development of a non-equimolar $AlCrCuFeNi$ high-entropy alloy and its corrosive response to marine environment under different temperatures and chloride concentrations. *J. Alloys Compd.* **2022**, *928*, 167112. [[CrossRef](#)]
70. Liu, C.; Liu, Z.; Gao, Y.; Zheng, C.; Wang, X. Investigation on the corrosion behavior of $Ni-Cr-Mo-W-xSi$ laser cladding coating in H_2S corrosion environment. *Appl. Surf. Sci.* **2022**, *578*, 152061. [[CrossRef](#)]
71. Thorhallsson, A.; Fanicchia, F.; Davison, E.; Paul, S.; Davidsdottir, S.; Olafsson, D. Erosion and corrosion resistance performance of laser metal deposited high-entropy alloy coatings at hellisheidi geothermal site. *Materials* **2021**, *14*, 3071. [[CrossRef](#)]

72. Wan, H.; Song, D.; Shi, X.; Cai, Y.; Li, T.; Chen, C. Corrosion behavior of $\text{Al}_{0.4}\text{CoCu}_{0.6}\text{NiSi}_{0.2}\text{Ti}_{0.25}$ high-entropy alloy coating via 3D printing laser cladding in a sulphur environment. *J. Mater. Sci. Technol.* **2021**, *60*, 197–205. [[CrossRef](#)]
73. Wang, Q.; Amar, A.; Jiang, C.; Luan, H.; Zhao, S.; Zhang, H.; Le, G.; Liu, X.; Wang, X.; Yang, X.; et al. CoCrFeNiMo_{0.2} high entropy alloy by laser melting deposition: Prospective material for low temperature and corrosion resistant applications. *Intermetallics* **2020**, *119*, 106727. [[CrossRef](#)]
74. Ben, Q.; Zhang, Y.; Sun, L.; Wang, L.; Wang, Y.; Zhan, X. Wear and corrosion resistance of FeCoCr_xNiAl high-entropy alloy coatings fabricated by laser cladding on Q345 welded joint. *Metals* **2022**, *12*, 1428. [[CrossRef](#)]
75. Chen, X.; Qian, H.; Lou, Y.; Yang, B.; Cui, T.; Zhang, D. Effects of Cu-content and passivation treatment on the corrosion resistance of $\text{Al}_{0.3}\text{Cu}_x\text{CoCrFeNi}$ high-entropy alloys. *J. Alloys Compd.* **2022**, *920*, 165956. [[CrossRef](#)]
76. Zhang, Z.; Yuan, T.; Li, R. Striped non-uniform corrosion behavior of non-equiatomic FeMnCoCr high-entropy alloy prepared by laser melting deposition in 0.1 M H_2SO_4 solution. *Materials* **2020**, *13*, 5554. [[CrossRef](#)]
77. Croll, S. Surface roughness profile and its effect on coating adhesion and corrosion protection: A review. *Prog. Org. Coat.* **2020**, *148*, 105847. [[CrossRef](#)]
78. Umoren, S.; Solomon, M. Protective polymeric films for industrial substrates: A critical review on past and recent applications with conducting polymers and polymer composites/nanocomposites. *Prog. Mater. Sci.* **2019**, *104*, 380–450. [[CrossRef](#)]
79. Aslam, R.; Mobin, M.; Zehra, S.; Aslam, J. A comprehensive review of corrosion inhibitors employed to mitigate stainless steel corrosion in different environments. *J. Mol. Liq.* **2022**, *364*, 119992. [[CrossRef](#)]
80. Zhang, P.; Xu, Z.; Yao, Z.; Liu, Y.; Lin, S.; He, M.; Lu, S.; Wu, X. A high-corrosion-resistant high-entropy alloys (HEAs) coatings with single BCC solid solution structure by laser remelting. *Mater. Lett.* **2022**, *324*, 132728. [[CrossRef](#)]